



NEW ZEALAND SOCIETY FOR EARTHQUAKE ENGINEERING
**2019 Pacific Conference on
Earthquake Engineering**
TURNING HAZARD AWARENESS INTO RISK MITIGATION
4 – 6 April | SkyCity, Auckland | New Zealand



Lateral instability of self-centring braces: buckling in loading and unloading

S.M.M. Yousef-beik & P. Zarnani

Auckland University of Technology, New Zealand, Auckland.

A. Hashemi & P. Quenneville

University of Auckland, New Zealand, Auckland.

ABSTRACT

The competitive advantage of the self-centring (SC) braces is that they have a predictable, reliable and identical flag-shape response both in tension and compression. A recent study shows that self-centring braces are vulnerable to buckling and showing unstable responses both in the loading and unloading phase when they are working in compression. Thus, if not controlled, this lateral instability can function as a major interrupting parameter, which can affect the brace performance. Up to authors' best knowledge, because this issue is not studied in the past literature, this paper attempts to discuss this problem further in detail and provide the experimental demonstration. In the first part, the analytical stability model for prediction of lateral instability of SC braces will be discussed, then it will be verified with a new self-centring brace equipped with Resilient Slip Friction Joint. According to the experimental observations, the buckling of these braces can interestingly occur either in loading or unloading phase and also can considerably affect the capacity of the brace in compression.

1 INTRODUCTION

The Pre-cast Seismic Structural Systems (PRESSSS) program was possibly the first study on using the rocking structures as new low-damage lateral load resisting system with a flag-shape response. In that program, precast post-tensioned rocking concrete walls were used together with U-shaped flexural plate to dissipate the input seismic energy (Priestley, Sritharan, Conley, & Pampanin, 1999). The concept is based on the idea that post-tensioned tendons provide the nonlinear elastic response while yielding flexural plates offer the required damping. Combination of these two mechanisms will form the flag-shape response. Extension of this concept for Moment-resisting Frames (MRFs) was studied by (Rojas et al. 2005), (Garlock et al. 2005) and (Christopoulos et al. 2002). Further study of the concept on bridge piers was conducted by

(Palermo et al. 2007). In another study, (Clayton et al., 2016) adopted such a concept for steel plate shear walls. (Buchanan et al. 2007) studied the application of U-shaped flexural plates (UFPs) in a post-tensioned LVL timber rocking walls and extend the PRESS concept in timber shear walls. Other researchers also studied and developed the combination of post-tensioned elements and additional friction dampers in steel self-centring braces and rocking steel braces (Christopoulos et al. 2008; Erochko et al. 2014; Erochko, Christopoulos et al. 2013).

Self-centring braces indeed are well-known for their repeatable and identical flag-shape response both in tension and compression (Christopoulos et al., 2008; Erochko et al., 2014; Erochko et al., 2013) unlike conventional concentrically braced frames in which each cycle has strength degradation due to inelastic buckling and formation of plastic hinge (Lee & Bruneau, 2005). A recent study shows that self-centring braces are also vulnerable to lateral instability (Hashemi et al., 2019; Yousef-beik et al. 2018) due to either a slender body or arrival of rotational flexibility along their length, which can be a damper. Due to this, the brace can prematurely fail due to exhibiting a large deflection to the side and not reaching its capacity. Such an analogous problem has been observed in the Buckling-restrained Braces (BRB). In these systems although the BRB is designed to yield in compression, it may fail prematurely if the gusset plates are not adequately designed (Takeuchi et al. 2014; Zaboli et al. 2018). In other words, the BRB and its gusset plates can buckle together before reaching its capacity in compression. In order to address this problem, some stability criteria based on buckling mode shapes, end connections and configurations of BRB have been put forth by (Hikino et al. 2012; Takeuchi et al., 2014). In a simple word, in BRBs, the gusset plates should be designed stiffer as compared those of conventional braces to ensure the stability of brace so that the global buckling does not occur before core yielding. The identical story can be generalized for RSFJ brace. This paper mainly discusses the buckling of self-centring braces with rotational flexibility along their length. Interestingly, there can be also a unique characteristic regarding buckling of SC braces, which is the possibility of buckling both in loading and unloading. The root cause of this is due to the restoring force, acting within the unloading path. It will be shown that if buckling takes place, the post-slip stiffness and compression capacity of the brace will noticeably reduce and possibly the performance of the brace may be interrupted. This paper attempt to present a method in order to analyse this instability and quantify the associated loads.

2 STABILITY MODEL

Similar to any compressive member, one of the main phenomena that may adversely affect the performance of a tension-compression brace is the buckling, which is normally known by premature fail due to increasing deflection to the side. Consider the following model for an intended SC brace along which there is a rotational flexibility (here is a damper).

If it is assumed that work done on the system is path-independent, the potential energy of the proposed model - including the effect of initial imperfections - during the loading phase is:

$$\pi(\theta) = \int_0^{\theta \leq \theta_{ult}} M(\theta) d\theta - PL_1 \left(\cos(\theta_1) - \cos(\theta_{0,1}) \right) - PL_2 \left(\cos(\theta_2) - \cos(\theta_{0,2}) \right) \quad (1)$$

Where the first term in the potential energy refers to strain energy conserved in the damper while the second and third terms refer to external work done by external axial load. It should be noted that in the calculation of potential energy, the brace bodies were assumed to be relatively rigid to damper, which is a reasonable assumption as the flexural stiffness of brace body is much higher than the post-slip rotational stiffness damper, so the energy conserved in the brace bodies can be neglected. Any one may argue that this is not a general case and may not be a conservative assumption if the brace bodies are slender. However, for further simplicity, this assumption was made. The effect of relative stiffness of brace body to damper is a relatively new subject, which requires further research.

Using stability analysis and Lagrange-Dirichlet theorem, stating that strict minimum of potential energy will bring the critical load (Bažant et al. 2010; Budiansky 1974), it can be shown that the critical load can be calculated by:

$$P_{cr,loading} = \frac{L \frac{d}{d\theta} \int_0^{\theta < \theta_{ult}} M(\theta)}{L_1 L_2} \quad (2)$$

Where “L”, “L₁” and “L₂” are defined in Figure 1 (a). If tangent stiffness of rotational spring is assumed to be

“ $K_{tan} = \frac{d}{d\theta} \left[\int_0^{\theta \leq \theta_{ult}} M(\theta) \right]$ ”, the critical load can be calculated as:

$$P_{cr,loading} = \frac{K_{tan} L}{L_1 L_2} \quad (3)$$

Same process can be followed for the unloading phase, and it can be concluded that critical loads associated with unloading are a function of associated post-reversed slip rotational stiffnesses.

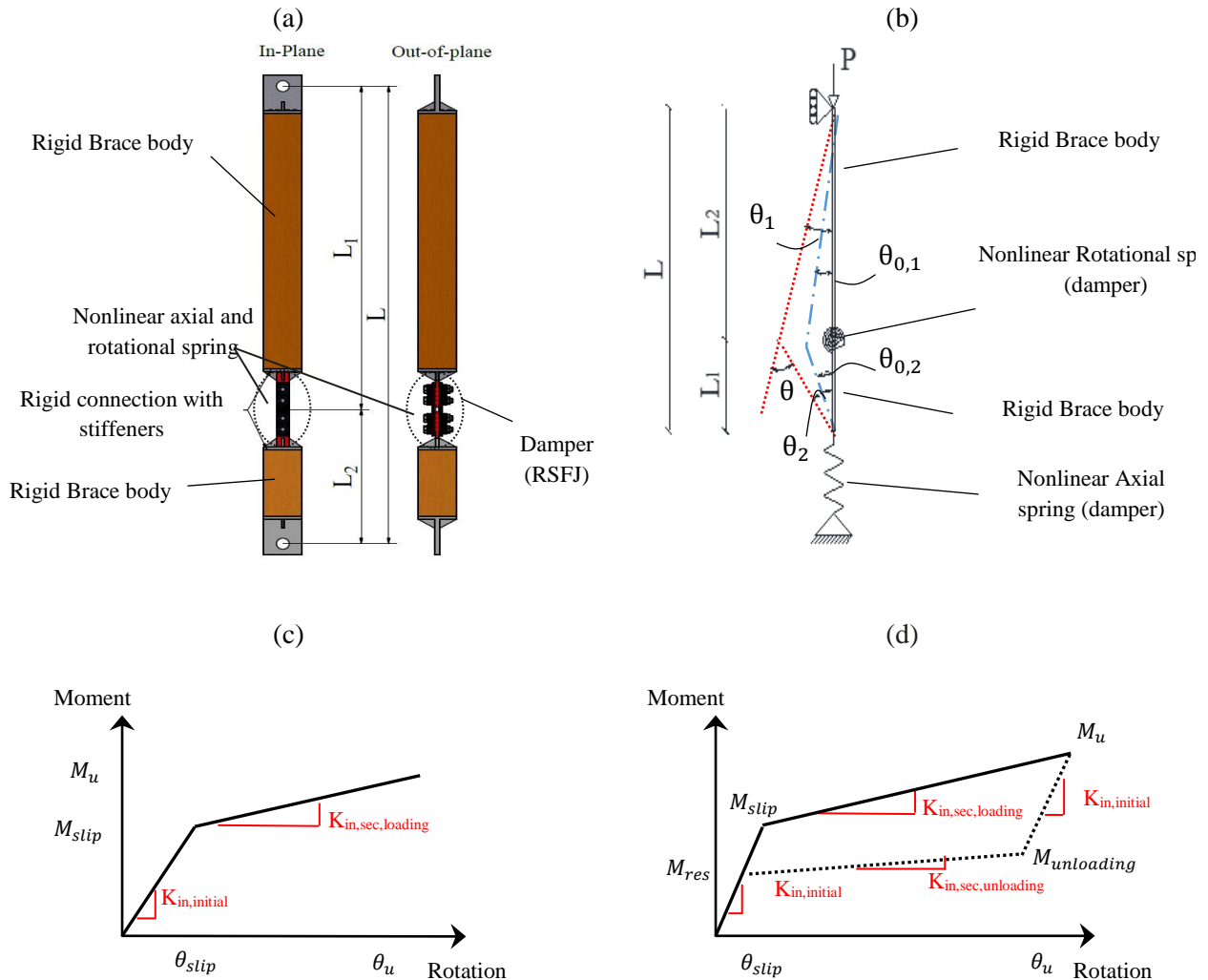


Figure 1: (a) intended brace configuration in-plane and out-of-plane (b) Proposed stability model for a SC brace with a rotational flexibility, (c) bilinear rotational spring (out-of-plane), (d) flag-shape rotational spring (in-plane),

Equation 2 indicates that the instability load of the brace is a function of tangent rotational stiffness of rotational spring. It is worth mentioning that the term “tangent” refers to the phase in which damper is acting. If damper is at before-slip phase, tangent rotational stiffness shall be regarded as initial rotational stiffness

(Figure 1(c, d)); however, if damper is activated, the tangent rotational stiffness shall be regarded as post-slip (secondary) rotational stiffness. Accordingly, for a system with bilinear rotational flexibility (Figure 1 (c)), there are two buckling loads namely before and after-slip associated with initial and post-slip phases while for a system with rotational flexibility with flag-shape response (Figure 1 (d)), there are three instability loads associated with before, after-slip (loading and unloading), respectively.

3 EXPERIMENTAL VERIFICATION WITH RSFJ BRACE

In order to verify the stability model, a scaled self-centring timber brace with rotational flexibility was designed and tested. In this brace, all the energy dissipation is supposed to be provided by the RSFJ damper (Zarnani & Quenneville, 2015) through axial movement of the damper, but as it has an in-plane and out-of-plane rotational flexibility, the brace is prone to buckle both in-plane and out-of-plane. The out-of-plane and in-plane performance of RSFJ damper is illustrated in Figure 1 (c, d).

In the following figure, axial performance of a RSFJ damper can be seen. This damper is able to provide a flag-shape response if it is loaded axially. For further information regarding its axial and rotational performance, it can be referred to (Hashemi et al., 2019; Yousef-beik et al.; Zarnani et al.).

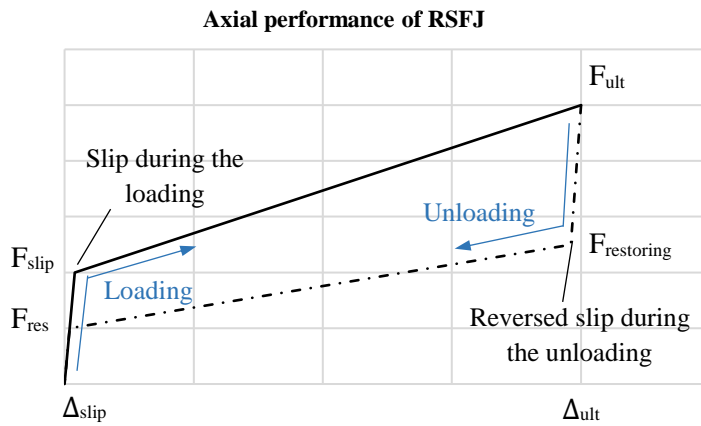


Figure 2: Axial Performance of RSFJ Damper

In this figure:

$$F_{slip} = 2n_b F_{pr} \left(\frac{\sin(\theta_g) + \mu \cos(\theta_g)}{\cos(\theta_g) - \mu \sin(\theta_g)} \right) \quad (4)$$

$$F_{res} = 2n_b F_{pr} \left(\frac{\sin(\theta_g) - \mu \cos(\theta_g)}{\cos(\theta_g) + \mu \sin(\theta_g)} \right) \quad (5)$$

Where “ n_b ” is the number of bolts, “ θ_g ” is angle of grooves, “ μ ” is coefficient of friction and “ F_{pr} ” is prestressing force in the springs (Figure 3). The ultimate and the restoring axial loads that a joint can experience (F_{ult} and $F_{restoring}$) can be computed by replacing “ F_{pr} ” by “ F_u ” – which is the resultant maximum force of the disc spring stack in its fully flat position – in the “ F_{slip} ” and “ F_{res} ” equations, respectively.

The only parameters that are required for stability analysis of the brace are the in-plane and out-plane rotational stiffness of RSFJ to be input as the nonlinear spring in the mathematical model (Figure 1(b)). Then based on equation 3, the associated buckling loads can be calculated. According to experimental observation, initial (before-slip) rotational stiffness is much higher than that of post-slip. Hence, the buckling with initial rotational stiffness during the before-slip phase is unlikely and not studied in this program. Equation 6 and Equation 7 shows the post-slip stiffness of RSFJ in in-plane direction for loading and unloading phase while Equation 8 shows the post-slip rotational stiffness of RSFJ in the out-of-plane direction (shown in Figure 1(c, d)). If these stiffnesses are replaced in Equation 3, the associated buckling loads can be carried out.

Paper 13 - Lateral Instability of Self-centring Braces: Buckling in loading and Unloading

$$K_{in,sec,loading} = n_b K_{st} \cdot b^2 \cdot \tan(\theta_g) \left(\frac{\sin(\theta_g) + \mu \cdot \cos(\theta_g)}{\cos(\theta_g) - \mu \cdot \sin(\theta_g)} \right) \quad (6)$$

$$K_{in,sec,unloading} = n_b K_{st} \cdot b^2 \cdot \tan(\theta_g) \left(\frac{\sin(\theta_g) - \mu \cdot \cos(\theta_g)}{\cos(\theta_g) + \mu \cdot \sin(\theta_g)} \right) \quad (7)$$

$$K_{out,sec} = n_b K_{st} \cdot \frac{l_e^2}{4} \quad (8)$$

Where “b” is width of cap plates, “ K_{st} ” is the stiffness of disc spring stack and “ l_e ” is overlap length between cap and middle plate. The assemblage of a RSFJ damper at different poses is depicted in Figure 3. As it can be observed, all of the post-slip rotational stiffnesses are directly dependent on stiffness of a stack and number of bolts. Moreover, the in-plane post-slip stiffness is directly correlated with width of cap plates while out-of-plane post-slip stiffness depends on overlap length between cap and middle plate.

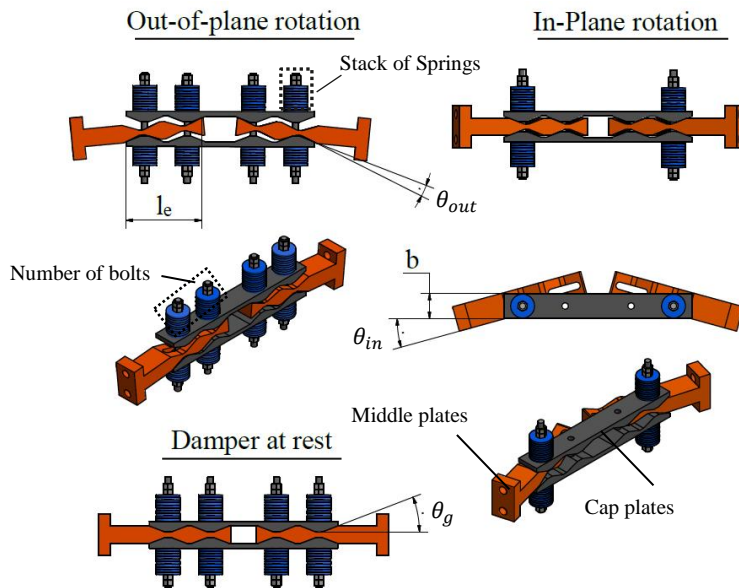


Figure 3: RSFJ damper at different poses plus related parameters

3.1 Experimental setup

Considering a scale factor of 1/2.4, this brace with a length of 1717 mm can be the representative of a frame with 3.3-meter height and 5-meter length with a converse V-type bracing configuration. The brace specimen was made up of two main sections. One timber body and one RSFJ damper. The timber part was composed of an LVL grade 11 with an elastic modulus of $E = 11$ GPa and a density of $\rho = 500$ kg/m³. Besides, it had a 150 mm wide square-shape cross-section. The timber body part had parallel to grain nominal tension and compression inelastic capacity of 740 kN and 910 kN, respectively (according to the Eurocode 5). There were two end bracket plates with a thickness of 20 mm with a pin hole in them to provide the pin ended situation for the brace (shown in Figure 4). The connection between the bearing plates and the timber column was capacity designed (with respect to the capacity of section) and a total number of 8 self-tapping screws with 180 mm length and 7 mm diameter were used for the attachment. An actuator with 300 kN force and 100 mm stroke capacity was utilized for this test. The schematic drawings of the brace and the test setup are illustrated in Figure 4. For the purpose of data acquisition, two displacement gauges were used at both sides of the RSFJ to measure the axial deformation of the specimen. Furthermore, two Linear Variable Differential Transformers (LVDTs) were employed along the height of the brace to record the lateral displacement. Different configurations including two different stacks with the different number of springs and pre-stressing forces were considered for the testing program (see table 1). It should be noted that the stiffness associated

with each stack - “ K_{st} ” for 6 and 8-disc springs - was 6.405 KN/mm and 4.292 KN/mm respectively according to experimental results (Yousef-beik et al.).

For this testing program, the following loading regime is employed. The continuous black line in Figure 5 is the main loading regime with a maximum of 9 mm indicative of 1.5% lateral drift (assumed to be the representative for the design level earthquake). As it can be seen in Figure 5, there is an additional part (dashed line) in the loading protocol for the compression part that is employed for the configuration 2 to further investigate the brace behaviour in compression after the Ultimate Limit State (ULS). This part has a maximum of 13.5 mm displacement - or 1.5 times bigger than 9 mm (the ULS level), equivalent to 2.25% lateral drift, which can be interpreted as the lateral drift in event of Maximum Considerable Earthquake (MCE).

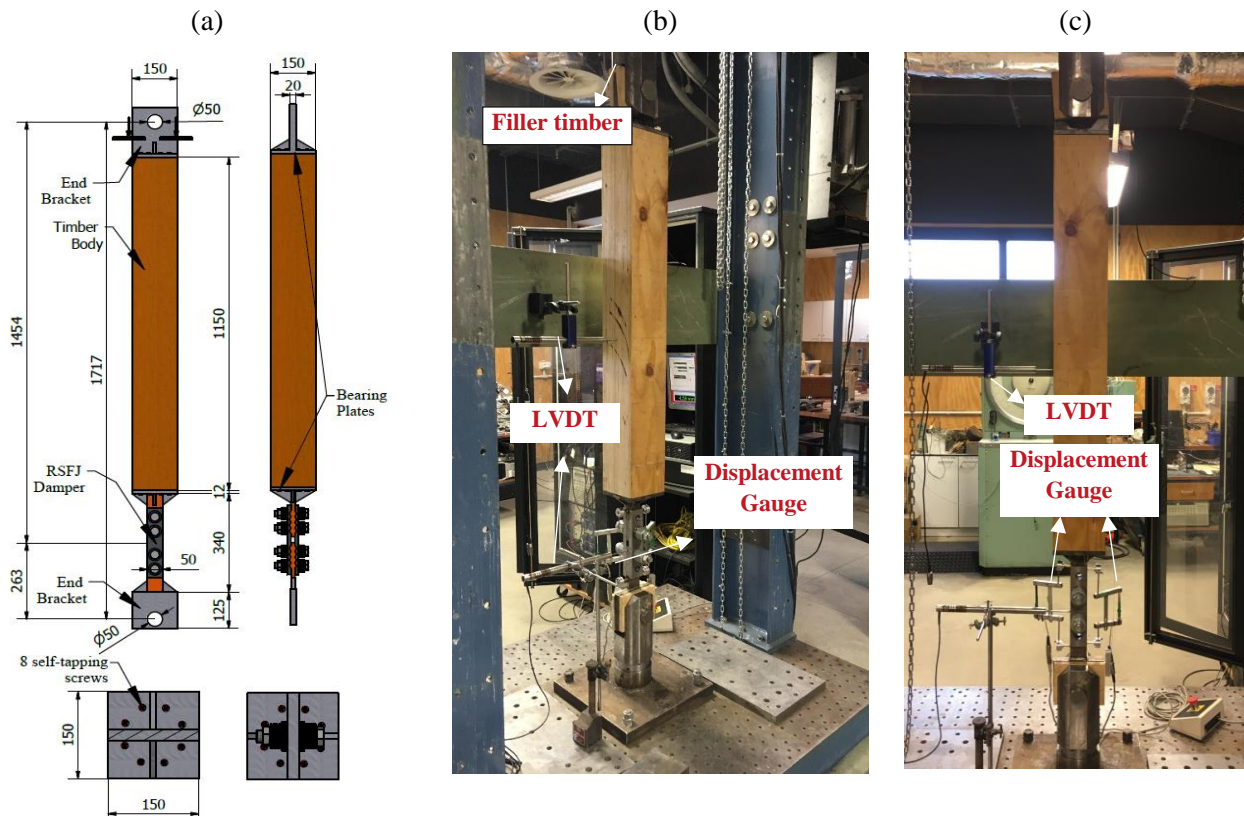


Figure 4: Test setup and specimen: (a) Side views of test specimen for the in-plane testing (b and c) Experimental test setup

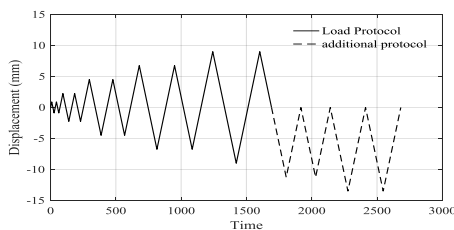


Figure 5: The loading protocol

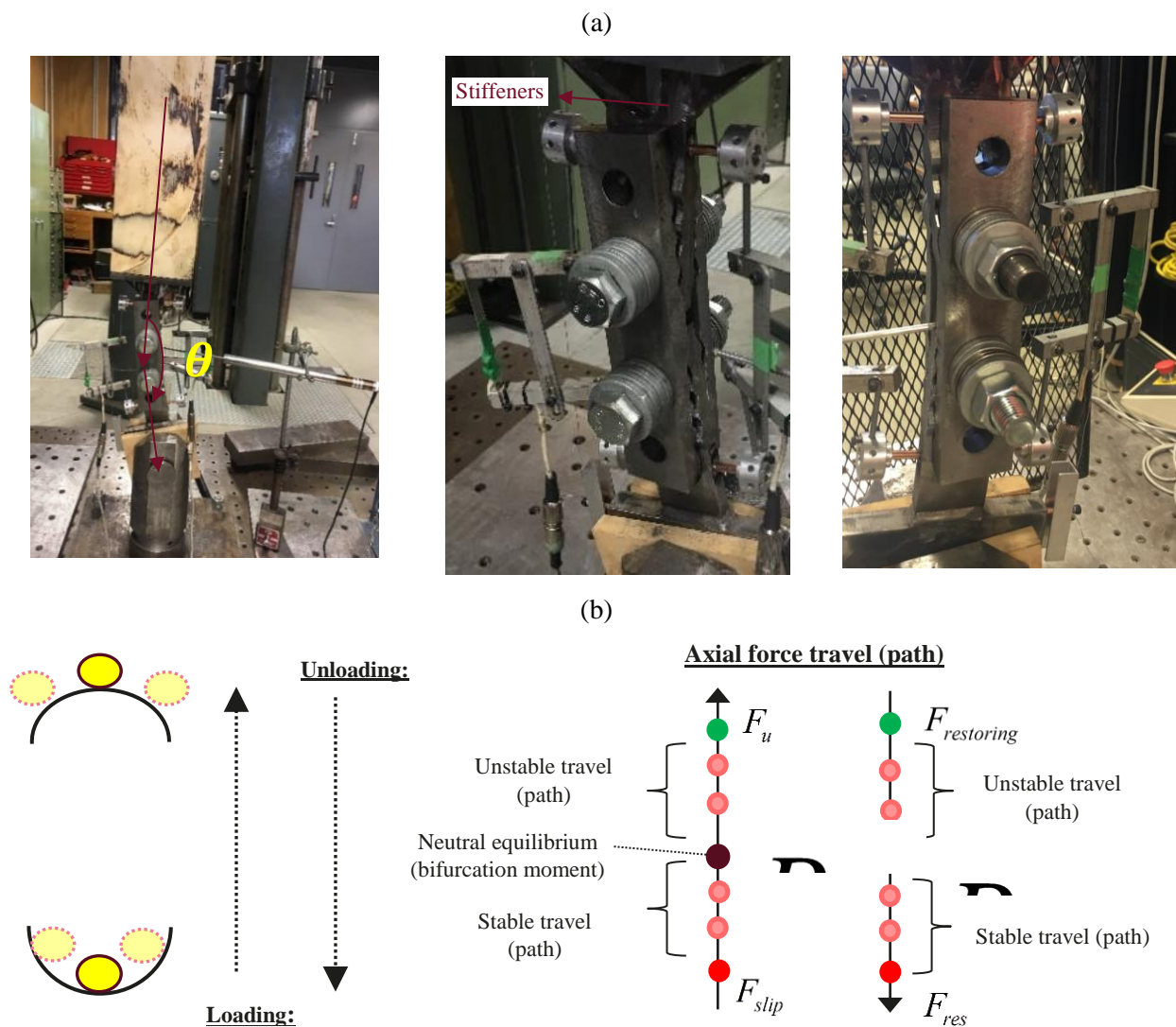
3.2 Experimental results

This section focuses on the evaluation of the proposed stability model for the configurations 1 and 2 shown in Table 1. The in-plane and out-of-plane post-slip rotational stiffness of damper is provided in Table 1. As *Paper 13 - Lateral Instability of Self-centring Braces: Buckling in loading and Unloading*

the in-plane rotational stiffness of the brace was lower than that of out-of-plane, the in-plane buckling global buckling load (see equations 3, 6-8) was higher than that of out-of-plane, and as a result the in-plane instability was governing (Hashemi et al., 2019). The flag-shape response hysteresis loops for configurations 1 and 2 are shown in Figure 6 (b and c). As can be observed, the tension parts of the experimentally obtained diagrams are in good agreement with the predicted analytical flag-shapes (the black dashed line) (Yousef-beik et al.). However, this is not true when it comes to the “compression part” due to buckling of the brace. The global buckling mode shape can be found in Figure 6 (a). The left figure depict the global buckling of brace while the other two depict the damper deformation during the global buckling. As it is clear, there is a relative rotation between middle plates and cap plates. It should be also noted that the connection of damper to timber bodies are stiffened with extra stiffeners in order to ensure rigid and robust connection, thereby cancelling out the effects of flexible connection.

Table 1: Test configurations

Configuration	n_d	γ (%)	F_{slip} (kN)	$F_{sresidual}$ (kN)	F_{ult} (kN)	$F_{restoring}$ (kN)	$K_{in,sec,unloading}$ (kN.m)	$K_{in,sec,loading}$ (kN.m)	EI_{body} (kN.m)	$P_{cr,loading}$ (kN)	$P_{cr,unloading}$ (kN)
1	6	15	9.1	4.4	32	15.6	1.8	3.7	247.5	17.5	8.5
2	8	27	16.4	8	31.6	15.4	1.21	2.48	247.5	11.7	5.7



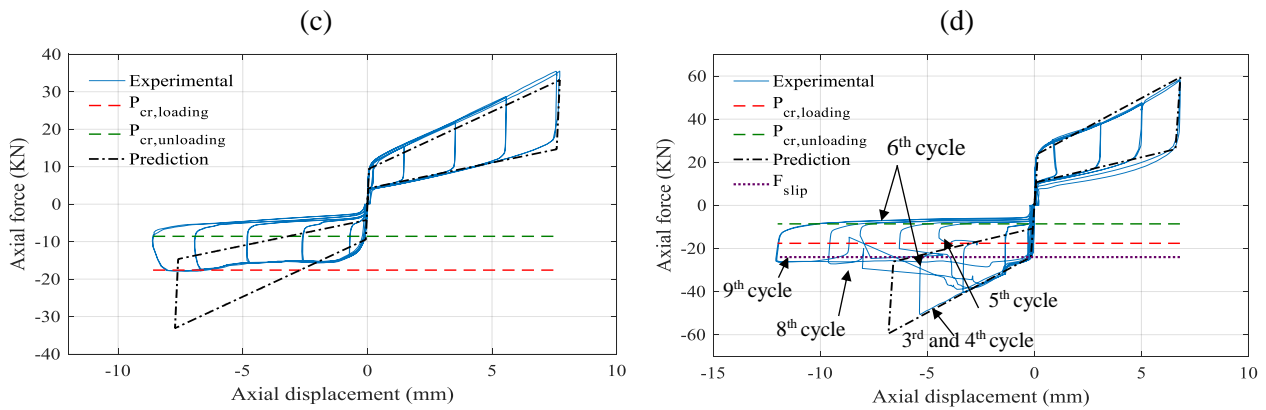


Figure 6: (a) the in-plane buckling mode shape for brace and damper, (b) hysteresis curve for configuration 1, (c) hysteresis curve for configuration 2

Figure 6 (b) describes the travel of axial load among different loading phases, which might be stable or unstable with respect to critical loads. Generally, if axial load is traveling within a zone upper than the critical load, SC brace is globally in an unstable condition, and a modest amount of deviation may result in instability. A simple analogy is made and shown in Figure (b) for a ball resting on a concave gravity surface. Nevertheless, if axial load is traveling within a zone lower than critical load, SC brace is globally in a stable condition, and any amount of deviation will be pulled back to initial position. A simple analogy is made and shown in Figure (b) for a ball resting on a convex gravity surface. In the vicinity of critical loads ($P_{cr,loading}$ or $P_{cr,unloading}$), situation is different. In fact, as the axial load is approaching and getting close to the critical load - either from upper or bottom zones-, the growth in deflection will accelerate. The important point is that the critical loads are the horizontal asymptote lines meaning that axial load may get very close or cross the buckling loads but never converges to it.

Figure 6 (c) depicts the experimental results of configuration 1. The slip force (F_{slip}) and the buckling force corresponding to loading ($P_{cr,loading}$) for this specimen were approximated to be 9.1 kN and 17.8 kN, respectively. As it can be seen, SC brace buckled in all cycles as soon as it approaches the “ $P_{cr,loading}$ ”. More specifically, it buckled from the moment that it reached the buckling load, and never experienced the flag-shape path beyond the buckling load. The flag-shape path beyond the critical load, also referred to as the secondary unstable path, is unstable as it is located in upper zone compared to the associated critical load.

Figure 6 (d) depicts the experimental results of configuration 2. In this configuration, behaviour of the brace got even more complex in the loading phase as the slip force (F_{slip}) was already higher than the buckling force corresponding to loading ($P_{cr,loading}$). So, possibility of global instability existed as soon as damper is activated. Interestingly, during the third and fourth cycles, the brace did not exhibit any instability although it partly exceeded the buckling load “ $P_{cr,loading}$ ” and entered the unstable zone. During the fifth cycle, an unexpected behaviour was observed for the brace. It strangely buckled when reaching to $P_{cr,loading}$ while it was within the unloading phase. This mode of buckling was classified as an unexpected mode and is still under investigation. During the sixth cycle, the axial load reached to a peak of 40 kN during the primary unstable path (beyond the instability load), then became unstable and dropped to $P_{cr,loading}$. As soon as the unloading began, the axial load dropped to $P_{cr,unloading}$ and followed the secondary (zero-stiffness) path to unload. Same happened in the eighth cycle. The axial load reached to a peak of 40 kN, but it suddenly dropped to $P_{cr,loading}$ as it was within the unstable zone. After this drop, the loading of the brace was continued, so an increase of the axial load to the slip force was observed. Similar behaviour was observed during the ninth cycle. In the last cycle; however, the system plateaued after reaching the slip force in

loading and continued to the end of loading then followed the secondary path (zero-stiffness) when was unloading. Overall, as it can be seen, there was a good agreement between the observed and predicted instability loads in loading and unloading, and it can be concluded that this model is valid for utilization as long as the brace bodies are relatively rigid as compared to damper.

4 FURTHER DISCUSSION

4.1 Global buckling Vs brace body inelastic buckling

Previously discussed buckling loads (Equation 2) were indeed elastic capacity of brace (not damper) in case of global buckling. This elastic capacity of the brace may be less or higher than the inelastic capacity of the brace body -which, itself, is a function of the brace body slenderness ($\frac{Max(L_1, L_2)}{r}$). The inelastic capacity of the brace body is suggested by design codes such AISC 360 (Design-AISC) or NZS 3404 (NZS 3404, 2007) for a body mad of steel or NZ3603 for a body made of timber. In the first case, if the elastic buckling load SC brace with damper is less than the capacity of the brace body (shown in Figure 1 (a, b)), the brace tends to buckle globally before reaching to inelastic capacity of brace body. However, if the elastic buckling is more than that of inelastic for brace body, the inelastic buckling of brace body is going to occur before global buckling. To shed more light on this, consider a Sc brace with a RSFJ with the relative position of damper $\delta = \frac{L_1}{L} = 0.15, 0.25$ and 0.5 . If the overlap length (l_e) is 550 mm, $b = 305$ mm, number of bolts and disks per side are 24 and 11 and stiffness of single disk is 75 KN/mm, the out-of-plane post-slip rotational stiffness will be $4.95 \text{ e}7$ KN.mm and the in-plane post-slip rotational stiffness is $0.397 \text{ e}7$ KN.mm according to Equations 6 and Equation 8. If the experimental tests are performed with different slenderness of the brace body and include the out-of-plane buckling (Hashemi et al., 2019), the following results are expected and compared to inelastic steel brace body suggested by AISC 360 (AISC, 2010) and NZS 3404 (NZS 3404, 2007).

In case of in-plane buckling (right diagram), it can be seen that for different location of damper, brace will globally buckle before that the brace body inelastically buckle. Furthermore, it can be seen that as the damper location moves toward the middle of the brace, global buckling load will decrease. Therefore, it is desirable to insert the damper as close as possible to end connection. On the contrary, in case of out-of-plane buckling (left diagram), as it can be observed, brace body inelastic capacity is less than global buckling load. This indicates that brace body will experience inelastic buckling before out-of-plane global buckling.

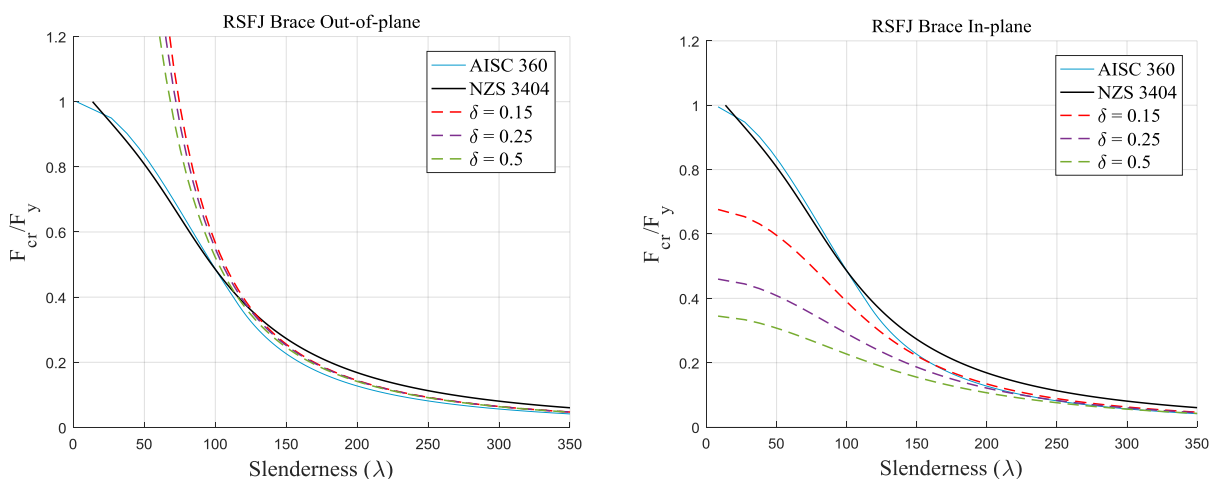


Figure 7: In-plane and out-of-plane buckling of RSFJ brace with respect to brace body slenderness

5 CONCLUSION

This paper discussed the possible buckling of self-centring (SC) braces with flag-shaped load-deformation response. Generally, these braces are prone to lateral instability both in loading and unloading. The main cause is that when these braces are working in compression, there is still a compressive force when they are unloading, which is due to their flag-shape response. If a phenomenon (like a sudden rotational weakness) reduces their rotational stiffness, this compressive force can trigger the lateral instability in unloading as well. As expected, the main consequence of buckling is that capacity of the brace in compression may reduce considerably and produce the unbalanced forces in connections. As it was shown in the experimental results, if the brace buckles in loading, it will follow the zeros stiffness path to unload.

6 ACKNOWLEDGEMENT

The authors would like to thank the Earthquake Commission (EQC) of New Zealand and the Ministry of Business, Innovation and Employment of New Zealand (MBIE) for the financial support provided for this research. The commercial interest for Tectonus company manufacturing RSFJ damper is acknowledged.

7 REFERENCES

- AISC. 2010. *AISC 360-10 Specification for Structural Steel Buildings*, Chicago, IL.
- Bazant, Z.P. & Cedolin, L. 2010. *Stability of structures: elastic, inelastic, fracture and damage theories*: World Scientific.
- Buchanan, A., Iqbal, A., Palermo, A. & Pampanin, S. 2007. Improved seismic performance of LVL post-tensioned walls coupled with UFP devices, *Proceedings of the 8th Pacific Conference on Earthquake Engineering*
- Budiansky, B. 1974. Theory of buckling and post-buckling behavior of elastic structures, *Advances in applied mechanics*, Vol 14 1-65.
- Christopoulos, C., Filiatrault, A., Uang, C.-M. & Folz, B. 2002. Posttensioned energy dissipating connections for moment-resisting steel frames, *Journal of Structural Engineering*, Vol 128(9) 1111-1120.
- Christopoulos, C., Tremblay, R., Kim, H.-J. & Lacerte, M. 2008. Self-centering energy dissipative bracing system for the seismic resistance of structures: development and validation, *Journal of Structural Engineering*, Vol 134(1) 96-107.
- Clayton, P.M., Dowden, D.M., Li, C.-H., Berman, J.W., Bruneau, M., Lowes, L.N. & Tsai, K.-C. 2016. Self-centering steel plate shear walls for improving seismic resilience, *Frontiers of Structural and Civil Engineering*, Vol 10(3) 283-290.
- Design-AISC 360-10 9 Steel Design-AISC 360-10. *Steel Design per AISC*, 360-310.
- Erochko, J., Christopoulos, C. & Tremblay, R. 2014. Design and testing of an enhanced-elongation telescoping self-centering energy-dissipative brace, *Journal of Structural Engineering*, Vol 141(6) 04014163.
- Erochko, J., Christopoulos, C., Tremblay, R. & Kim, H.J. 2013. Shake table testing and numerical simulation of a self-centering energy dissipative braced frame, *Earthquake engineering & structural dynamics*, Vol 42(11) 1617-1635.
- Garlock, M.M., Ricles, J.M. & Sause, R. 2005. Experimental studies of full-scale posttensioned steel connections, *Journal of Structural Engineering*, Vol 131(3) 438-448.
- Hashemi, A., Yousef-Beik, S.M.M., Darani, F.M., Clifton, G.C., Zarnani, P. & Quenneville, P. 2019. Seismic performance of a damage avoidance self-centring brace with collapse prevention mechanism, *Journal of Constructional Steel Research*, Vol 155 273-285.
- Hikino, T., Okazaki, T., Kajiwar, K. & Nakashima, M. 2012. Out-of-plane stability of buckling-restrained braces placed in chevron arrangement, *Journal of Structural Engineering*, Vol 139(11) 1812-1822.
- Lee, K. & Bruneau, M. 2005. Energy dissipation of compression members in concentrically braced frames: Review of experimental data, *Journal of Structural Engineering*, Vol 131(4) 552-559.
- Standards New Zealand. 2007. *NZS 3404: 1997 Part 1 and 2*. Wellington.
- Palermo, A., Pampanin, S. & Marriott, D. 2007. Design, modeling, and experimental response of seismic resistant bridge piers with posttensioned dissipating connections, *Journal of Structural Engineering*, Vol 133(11) 1648-1661.
- Priestley, M.N., Sritharan, S., Conley, J.R. & Pampanin, S. 1999. Preliminary results and conclusions from the PRESSS *Paper 13 - Lateral Instability of Self-centring Braces: Buckling in loading and Unloading*

- five-story precast concrete test building, *PCI journal*, Vol 44(6) 42-67.
- Rojas, P., Ricles, J. & Sause, R. 2005. Seismic performance of post-tensioned steel moment resisting frames with friction devices, *Journal of Structural Engineering*, Vol 131(4) 529-540.
- Takeuchi, T., Ozaki, H., Matsui, R. & Sutcu, F. 2014. Out- of- plane stability of buckling- restrained braces including moment transfer capacity, *Earthquake engineering & structural dynamics*, Vol 43(6) 851-869.
- Yousef-beik, S.M.M., Zarnani, P., Mohammadi, F., Darani, A.H. & Quenneville, P. 2018. New Seismic Damage Avoidance Timber Brace Using Innovative Resilient Slip Friction Joints for Multi-story Application, *Word Conference on Timber Engineering*, WCTE 2018, Seoul, Korea.
- Zaboli, B., Clifton, G. & Cowie, K. 2018. BRBF and CBF gusset plates: Out-of-plane stability design using a simplified Notional Load Yield Line (NLYL) method, *SESOC Journal*, Vol 31(1) 64.
- Zarnani, P. & Quenneville, P. 2015. *A Resilient Slip Friction Joint*. N. I. Office.
- Zarnani, P., Valadbeigi, A., Hashemi, A., Darani, F.M., Yousef-beik, S.M.M., Bagheri, H. & Quenneville, P. 2018. Rotational Performance of SlipFriction Joint (RSFJ) As a New Damage Free Seismic Connection, *Word Conference on Timber Engineering*, WCTE 2018, Seoul, Korea.